The Role of Porosity in Fatigue of PM Materials

Michael Andersson

Höganäs AB

Abstract

In this paper it's studied how density influences fatigue strength of two sintered steels; one standard, diffusion alloyed material and one sinter hardened pre alloyed chromium material. Fatigue testing on materials at different densities are performed and compared. Furthermore, extreme value statistics is applied to the pore structure to determine the size of the largest pore, and fracture mechanics is used to link fatigue strength to porosity. It's found that there is a strong correlation between fatigue limit and largest pore size. For the sinter hardened material it's found that a LEFM model can be used to predict fatigue crack initiation, whereas for the diffusion alloyed material with a complex microstructure initiation is a more complex interaction between porosity and the softer micro constituents.

Keywords

fatigue, fracture mechanics, porosity, extreme value statistics

Introduction

Compacted and sintered powder metallurgical materials provide a cost efficient solution for a wide range of applications. And as these materials and processes improve they can be applied to components with tougher and tougher requirements.

PM materials are by nature porous and the porosity will have a major influence on the mechanical properties of the material. Traditionally mechanical properties of PM materials are thought of as a function of density, and the means to get higher fatigue strength is to increase density. This, however, gives a very incomplete picture of what's actually happening in the material and in [1] it was demonstrated how fatigue strength can be increased by decreasing the size of the pores, keeping density constant, in this case by using powders of different sizes. The importance of porosity for fatigue strength is also addressed in by Bergmark in [2].

Typically fatigue cracks tend to initiate at the largest pore in a stressed volume. To investigate the connection between porosity and fatigue strength the size of the largest pore must thus be modelled. A useful tool for analysis of the influence from i.e. inclusions on the fatigue of classic steels is extreme value statistics, see i.e. Murakami [2]. Extreme value statistics can be used to model rare events and as fatigue tend to be controlled by the extremes, i.e. the largest inclusion, this methodology is well suited. It has also been used to study porosity in PM steels, cf. [1] and Beiss [4].

In this paper it's studied how density influences fatigue strength of two sintered steels; one standard, diffusion alloyed material and one sinter hardened pre alloyed chromium material. Fatigue testing on materials at different densities are performed and compared. Furthermore, extreme value statistics is applied to the pore structure to determine the size of the largest pore, and fracture mechanics is used to link fatigue strength to porosity.

Presented at DFPM in Stará Lesná, Slovak Republic, November 6 – 9, 2011

Modelling

The basic assumption for the model presented in this paper is that fatigue cracks start at the largest pore in the stressed volume, this means that the size of the largest pore must be estimated. The size of this pore can then be linked to the fatigue strength of the material. An often used tool to analyze defects in materials is extreme value statistics. This procedure is adopted here as well to analyse the porosity of the material. Then, by treating the pore as a sufficiently sharp notch, a fracture mechanics model is used to link pore size to fatigue strength.

Porosity analysis

To analyse the porosity a distribution function need to be fitted to the measured pore sizes. There are several extreme value distributions and no clear reason to chose one over another. Often the Gumbel distribution is used to analyse defects in materials and it will be used here as well. The distribution function is given by:

$$F_{Gum}(x) = \exp\left[-\exp\left(-\frac{x-\lambda}{\delta}\right)\right] \quad (1)$$

with the two parameters λ and δ. The distribution function can be rewritten as:

$$y = -\ln(-\ln F) = \frac{x-\lambda}{\delta} \quad (2)$$

which gives a linear relation that can be used to fit the parameters λ and δ to experimental results.

The Gumbel distribution occurs naturally when taking the maximum of a set of exponentially distributed stochastic variables, i.e. if

$$X_i \in \mathrm{Exp}(\theta) \quad (3)$$

and

$$Y = \max\{X_1, X_2, \ldots, X_N\} \quad (4)$$

the distribution of Y is given by

$$F_Y(x) = \left[F_x(x)\right]^N \quad (5)$$

and it can be shown that

$$Y \in \mathrm{Gum}\left(\frac{\ln N}{\theta}, \frac{1}{\theta}\right) = \mathrm{Gum}(\lambda, \delta) \quad (6)$$

The experimental procedure to estimate the parameters in the Gumbel distribution of the largest pore area for a material is to divide the cross section into a number of sub areas, with area, A_0, as illustrated in Figure 1. Each sub area is scanned with an optical microscope and through image processing software the area of each pore is measured and the area of the largest pore recorded. Max pore area is denoted x_i and they are sorted according to $x_1 < x_2 < \ldots < x_N$, with N being the total number of sub areas.

The corresponding F_i is calculated by see i.e. [2]

$$F_i = \frac{i}{N+1} \quad (7)$$

and the corresponding y_i is given by equation (2). This equation is also used to make a least squares fit to calculate λ and δ.

Since the largest pore in the stressed *volume* needs to be estimated the scanned cross section *area*, A_0, must be translated into a volume. In [2] a procedure is suggested where

$$V_0 = A_0 \cdot \frac{1}{N} \sum_i \sqrt{x_i} \tag{8}$$

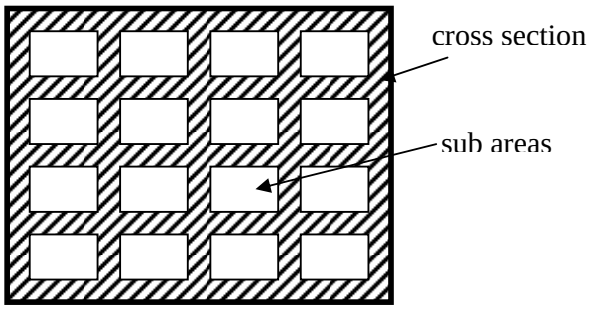

Figure 1. Cross section of a test bar divided into sub areas.

I.e. the depth of the volume is approximated as the average of the square root of the maximum pore areas. This is an empirical formula that has been proven useful and it will also be used here.

The resulting parameters give the distribution of the largest pore in the scanned volume and to translate this distribution to the stressed volume of a specimen it's assumed that the total number of pores in a volume is proportional to that volume. From equation (5) it then follows that the largest pore distribution function in volume V is given by

$$F_V(x) = \left[F_{V_0}(x) \right]^{\frac{V}{V_0}} = \exp\left[\frac{V}{V_0} \exp\left(-\frac{x-\lambda}{\delta} \right) \right] \tag{9}$$

where F_{V0} is the distribution function for the scanned volume.

To determine the largest pore in a given volume this equation can be rewritten into

$$A_\alpha = \lambda + \delta \left[\ln \frac{V}{V_0} - \ln\left(-\ln \alpha \right) \right] \tag{10}$$

where A_α is the largest pore with probability α. I.e. to determine the median average pore α=½.

Figure 2 shows two simulated Gumbel plots of y versus x. These were created by taking the maximum of a number of exponentially distributed points as given by the equations above. These curves show that even under ideal conditions points in the upper part of some curve (series 2) there are deviations from the expected Gumbel distribution. This will be used when evaluating the experiments where some data point will be excluded from the regression analysis.

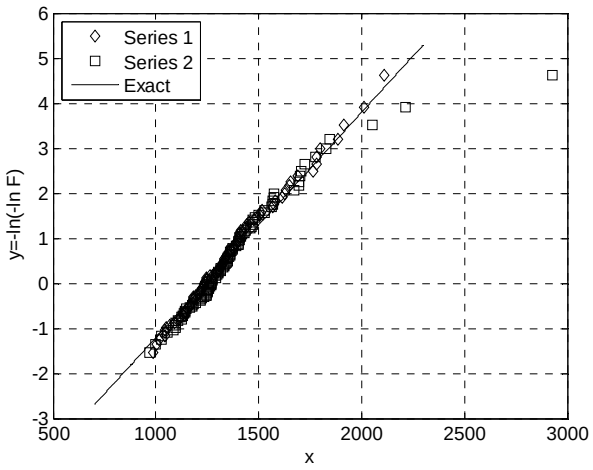

Figure 2. Two simulated Gumbel distributions along with the expected line.

A fracture mechanics model

By assuming fatigue crack initiation from the largest pore and considering that the pore is sufficiently sharp fracture mechanics can be used to calculate the fatigue limit of the material. Applying linear elastic fracture mechanics means that loading of a crack can be characterized by the stress intensity factor range, expressed as

$$\Delta K_I = \Delta\sigma\sqrt{\pi a}\cdot Y \qquad (11)$$

where $\Delta\sigma$ is the applied stress range, a crack length and Y a geometry factor. Below a certain threshold, ΔK_{th} cracks are assumed not to grow, meaning that the fatigue limit can be expressed as

$$\Delta K_{Iw} = \Delta K_{th} \qquad (12)$$

or by combining the equations

$$\Delta\sigma_w = \frac{\Delta K_{th}}{\sqrt{\pi a}\cdot Y} \qquad (13)$$

In the following it will be more convenient to work with crack area rather than crack length, and by taking the stress range as the stress amplitude by inferring no crack opening at negative stresses for R=-1 the following equation is obtained

$$\sigma_w = \frac{\Delta K_{th}}{B\cdot A^{\frac{1}{4}}} \qquad (14)$$

with A being crack area, here equivalent to largest pore are area, and B a constant accounting for crack and specimen geometry.

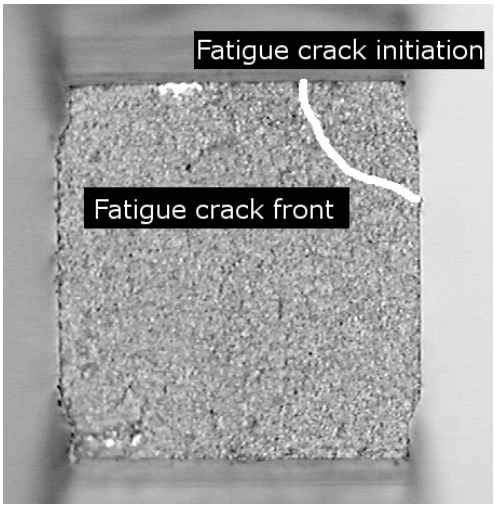

Figure 3. Crack initiation from the corner.

From experience, see Figure 3 and also the discussion by Bergmark in [2] it is known that cracks typically initiate in the corners of the specimens. Also, the exact crack shape tends to be of secondary importance [2]. Thus initiation is assumed to take place at a quarter circle located in the specimen corner, implying Y=0.722 [5]. Combined this results in B=1.36 and

$$\sigma_w = \frac{\Delta K_{th}}{1.36 A^{\frac{1}{4}}} \tag{15}$$

Taking ΔK_{th} as a constant predicts

$$\Delta\sigma_w \propto A^{\frac{-1}{4}} \tag{16}$$

Murakami [2] has suggested the following relation for crack growth threshold

$$\Delta K_{th} = 3.3 \cdot 10^{-3} \frac{H_V + 120}{A^{\frac{1}{6}}} \tag{17}$$

with H_V denoting the Vickers hardness. This equation suggests a fatigue threshold dependent on crack size and it leads to the well known Murakami expression for the fatigue limit where

$$\sigma_w \propto A^{\frac{-1}{12}} \tag{18}$$

Experimental

Materials

Two materials are included in this study; a pre alloyed chromium material, Astaloy CrM, and a diffusion alloyed material, Distaloy AE. Both materials were sintered at 1120°C in 90/10 N_2/H_2, with an addition of 0.2% CH_4 for CrM to avoid decarburization of the suface, for 30 min. The chromium material was subsequently sinterhardened with 2.5K/s. To produce different pore structures both materials were tested at different densities. A summary of the materials and processing conditions are given in Table 1.

Table 1. Materials

Designation	Material	Densities [g/cm^3]	Sintering	Cooling rate
AE	Distaloy AE (Fe+0.5%Mo+4%Ni+1.5%Cu)+0.6% C-UF4+0.6%Kenolube	{7.0, 7.2}	1120°C, 30 min, 90/10 N_2/H_2	≈0.8K/s
CrM	Astaloy CrM (Fe+0.5%Mo+3%Cr)+0.45%C-UF4+0.8%Amide wax	{6.9, 7.0, 7.15}	1120°C, 30 min, 90/10 N_2/H_2+0.2%CH_4 Tempering 200°C, 60 min	2.5K/s

The resulting microstructures are shown in Figure 4a and b. CrM displays fully martensitic microstructure after sinter hardening. Distaloy AE has a mixed, heterogeneous microstructure containing martensite, bainite, pearlite, ferrite and austenite, which is typical for diffusion alloyed materials with high alloying content.

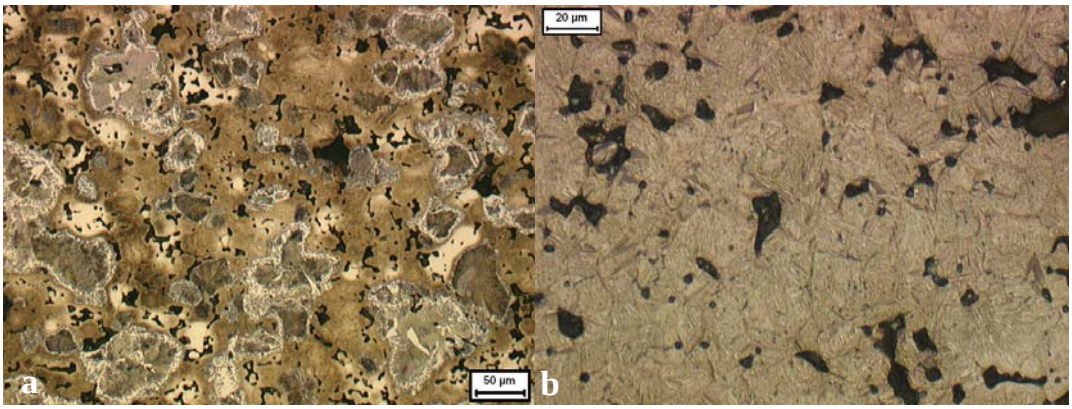

Figure 4. Microstructures for a. AE and b. CrM.

Porosity analysis

To do the extreme value analysis of the porosity a cross section perpendicular to the loading direction is cut from a test bar and polished. The piece of a test bar is then places in a microscope with a coordinate table and an automatic system used to scan section by section of the part. In each subsection the area of the largest pore is determined using image processing. A magnification of 20× was used giving an area of 0.278 mm^2 to the sub sections, and 50-80 subsection depending on how the specimen was mounted. Other magnifications (10× and 50×) have also been tried but 20× gave the best trade of between a large number of pores (hundreds) in the subsection and a fairly large number of sections.

After scanning the parameters λ and δ were calculated by a least squares fit to equation (2) calculating F_i according to equation (7). The resulting curves are shown in Figure 5. As can be seen a higher density moves the curve to the left, indicating smaller pores. In general the measured points correlate well with a Gumbel distribution, illustrated by the fact that they are more or less straight lines when plotting x versus y. However, there are a few points at the upper part of the curve that tend to deviate. This behaviour was also found in Figure 2 when the curves were created under ideal conditions. Thus it's believed that the Gumbel distribution is a good approximation of the actual max pore size distribution and the upper points are excluded from the least squared fit to provide a better correlation.

Apart from the distribution parameters the size of the scanned volume, V_0, was also calculated using equation (8). Then, from the estimated λ, δ and V_0, A_α were calculated using equation (10) with α=0.5 to get the median value of the largest pore. Figure 6 shows max pore area for the two sets of materials plotted against density. It's clear that a higher density corresponds to smaller largest pore. It's also seen that for a given density the largest pores in AE are approximately 1.5 times larger than in CrM. This difference is currently not understood, but need to be further investigated.

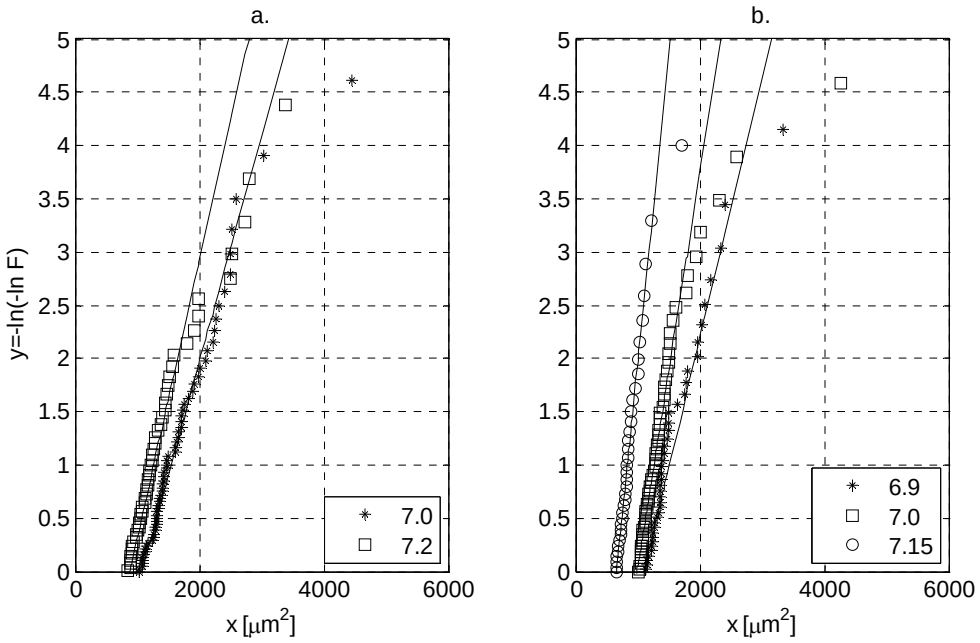

Figure 5. Gumbel distributions for a. AE and b. CrM.

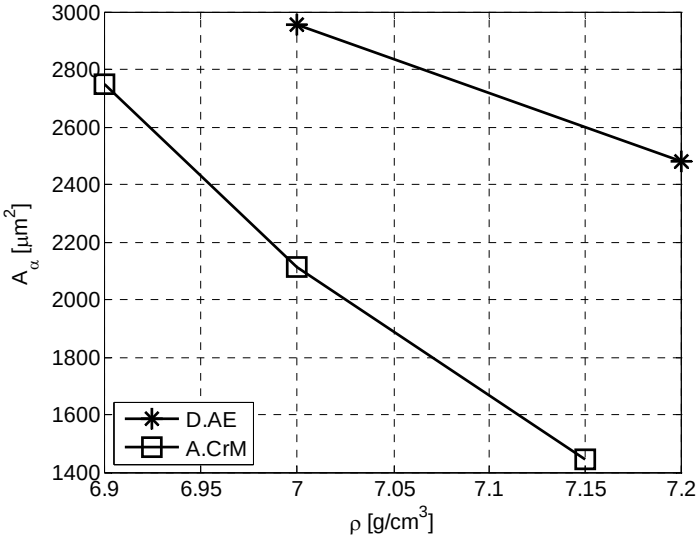

Figure 6. Max pore are plotted against density.

Fatigue testing

Fatigue testing was done in displacement controlled plane bending and a load ratio of R=-1. The test bars are ISO3928 sintered fatigue bars, with 5×5 mm^2 cross section. The geometry

was modified with a corner chamfer, as can be seen in Figure 3. Before testing, the corners of each specimen were carefully ground to remove burr from pressing. Testing was done using the staircase method, as described in MPIF Standard 51 [6], with 20-25 test bars in each series. The run out limit was set to $2 \cdot 10^6$ cycles, a specimen was considered a broken when containing a fatigue crack approximately 1 mm in length.

Fatigue strength as a function of density is plotted in Figure 7 for the two materials, fatigue strength is given as fatigue limit with 50% survival rate. As can be seen fatigue strength increases with increasing density. Also, the CrM has a higher fatigue strength than AE for a given density, due to the harder microstructure.

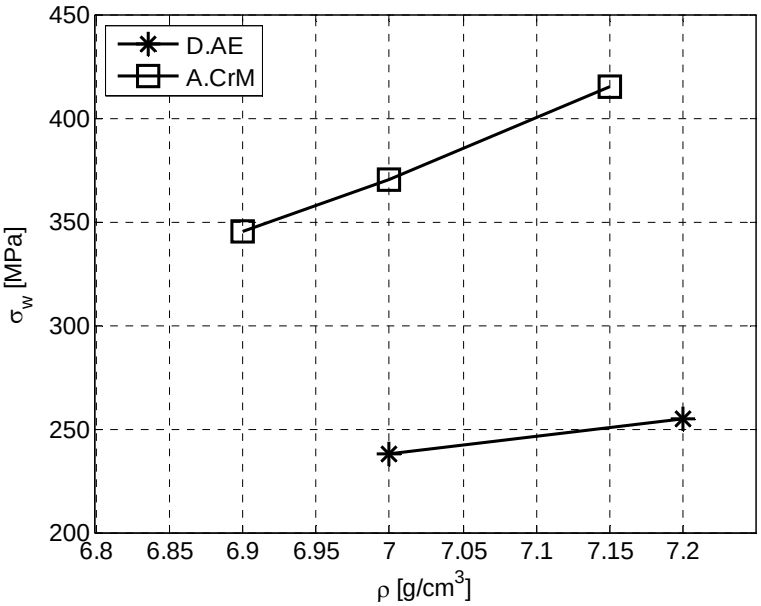

Figure 7. Fatigue strength as a function of density.

Fatigue strength and porosity

Next step is to investigate the relation between fatigue strength and pore structure. The assumption is that fatigue cracks start at the largest pore in the critical volume, and the porosity is represented by the expected largest pore in this volume. As critical volume the volume with at least 90% of the peak stress is taken in accordance with [2] or Sonsino [7].

Figure 8 shows the relation between endurance limit σ_w and largest pore A_{50}, note that the diagram has log-log scales. By making regression analyses of the data points the slopes of the curves can be calculated. This corresponds to the exponent, n, in a relation of the type:

$$\sigma_w = CA^n \qquad (19)$$

The resulting exponents are n_{CrM}=-0.29 and n_{AE}=-0.39. Linear elastic fracture mechanics predicts an exponent n=-0.25, as demonstrated above, which is close to the measured value for CrM. The Murakami model suggests n=-0.083, see above. In Figure 8 the regressions lines assumin n=-0.25 have been plotted. As can be seen they correlate well to the experimental data. From these lines the corresponding threshold values can be calculated from equation (15), giving ΔK_{th}=3.4 MPa$\sqrt{m}$ and 2.4 MPa$\sqrt{m}$ for CrM and AE respectively.

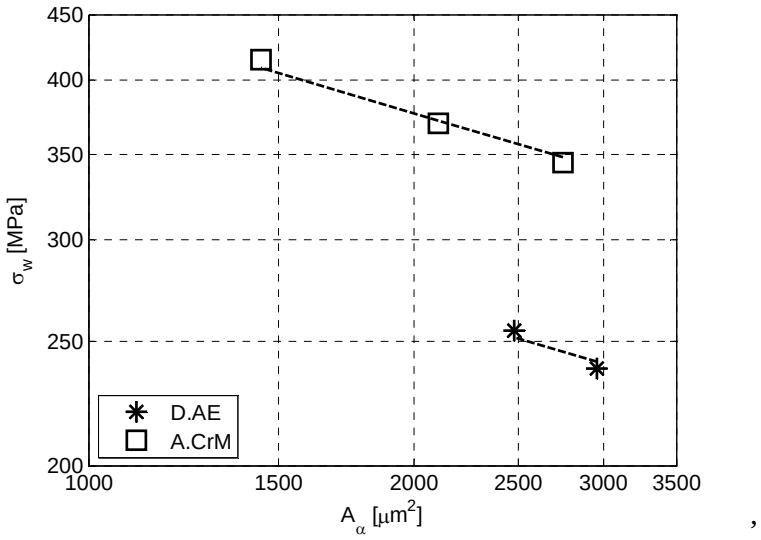

Figure 8. Fatigue limit as a function of largest pore size.

Discussion

It's clear that there is a strong correlation between higher density and a smaller size of the largest pore in PM materials. This also helps explain why a higher density leads to higher fatigue strength if it's assumed that fatigue crack initiation takes place at the largest pore in the stressed volume.

By plotting the fatigue limit against the size of the largest pore it's found that there is a good correlation with a power law as suggested by equation (19). The calculated exponents are n_{CrM}=-0.29 and n_{AE}=-0.39, which should be compared to n=-0.25 obtained from linear fracture mechanics combined with a constant fatigue threshold. For AE the exponent was calculated with only two data point giving a high degree of uncertainty to the estimate. By forcing the exponent to -0.25 it can be seen from Figure 8 that there is still a good correlation for both materials, and LEFM seems to provide a useful model.

The premise for using linear fracture mechanics is that the plastic zone ahead of the crack is sufficiently small. Max plastic zone at the fatigue limit can be estimated from

$$r_p = \frac{1}{3\pi}\left(\frac{\Delta K_{th}}{\sigma_{ys}}\right)^2 \qquad (20)$$

where σ_{ys} is the yield stress. The macroscopic yield stresses at 7.0 g/cm^3 are approximately 900 MPa for Astaloy CrM and 450 MPa for Distaloy AE in the tested conditions [10].

Using the estimated ΔK_{th} from above and the macroscopic yield strengths this translates to plastic zones of 1.5μm for CrM and 3μm for AE. Crack lengths are roughly 40-50μm, i.e. more than 20 times longer than the plastic zone.

As the macroscopic yield strength are dependent on the stress concentrations around the pores the microscopic yield strength ahead of the material can be expected to be higher for the homogenous structure of CrM and thus the plastic zone small compared to the crack length.

Distaloy AE is more complicated due to the heterogenous structure with soft constituents such as ferrite and austenite. If the microscopic yield strength in the soft points are half the

macroscopic value the plastic zone will increase to 12µm, which is in the same order of magnitude as the crack length.

Thus for the hard structure of CrM linear fracture mechanics is a valid approach, but for AE with softer parts of the structure the plastic zone is large and LEFM may not be accurate.

From curve fitting, combined with a fracture mechanics model the corresponding measured threshold values were also calculated. For CrM ΔK_{th} is found to be 3.4 MPa√m, which is within the range ΔK_{th}=3.4..4.6 MPa√m that was found by Yu and Topper [8] for different martensitic microstructures. The fact that the obtained value is in the lower range can be explained by the low carbon content (0.45%) in the tested material. The measured value for AE was ΔK_{th}=2.4 MPa√m, a non hardened steel can be expected to have a threshold around 6 MPa√m cf. Frost et.al. [9], which is considerably higher.

The conclusion is that the LEFM model seem valid for hard microstructures, which is also found in Figure 1, and could in principle be used to predict the fatigue strength for these materials.

The heterogeneous structure of AE with soft constituents make the situation more complex. It's also known that crack initiation in heterogeneous PM materials often take place in the softer phases, i.e. the pores typically play a minor role Alzati et.al. [11]. This fact, combined with the low measured value for ΔK_{th} makes the presented model questionable for these materials. Materials with such heterogeneous structures probably need more sophisticated models, accounting for both pore and microstructure and the interactions between them.

In [2] the stress intensity factor is formulated in terms of the convex crack area. In this paper actual crack area is used instead. The reason being that convex area for very slender pore structures, as illustrated in Figure 9a, are significantly larger that the pores with largest actual area, see Figure 9b. However, the significant dimension of the slender structures are the width of the crack and then using convex area gives an erroneous measure of stress intensity. On the other hand using actual area will give a lower stress intensity factor than with convex area for the same pore, but this error is considered minor.

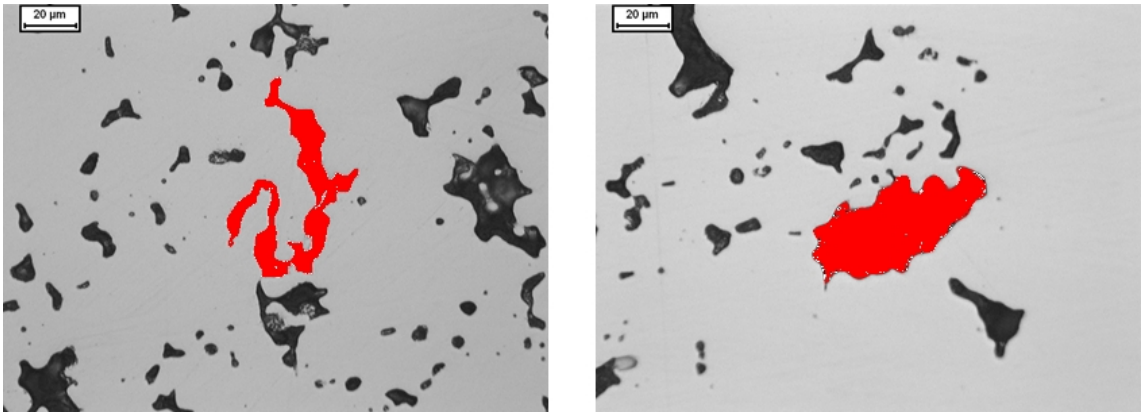

Figure 9. a. slender pore with large convex area, b. rounder pore with convex area close to actual area.

There is no physical reason for choosing the Gumbel distribution over some other extreme value distribution other than that it seems to be in good agreement with the measured distributions. Looking at the experimental curves in Figure 5 it's seen that the correlation between the experimental data and distribution function is good except from the upper part of the curve. In principle a general extreme value distribution could be used to incorporate this behaviour in the model, see i.e. [13]. However, the deviations from a straight line in the upper

part of the curve are consistent with the behaviour obtained in the simulations, Figure 2, which was obtained from conditions that should give an ideal Gumbel distribution. Thus this behaviour could just as well be a result of the statistical method and limited set of data used and it does not seem meaningful to use another distribution.

The presented model can in principle be used to predict the full distribution of the fatigue limit, i.e. not only the median value, by assigning different values to α in equation (10). The assumption is then that scatter in fatigue strength is dominated by the scatter in initiation defects. Using a given extreme value distribution will then automatically give a corresponding distribution for the fatigue limit. At the same time it is normally assumed, although it's rarely possible to test, that the fatigue limit follows a normal distribution, and this is also used for evaluating staircase data. Around the median value the error is probably not too great but trying to predict i.e. values around the lower tail of the distribution it will be a critical matter. A more detailed discussion on the matter along with a suggestion for a distribution for the fatigue limit consistent with the Gumbel defect distribution can be found in Svensson et.al. [12].

Conclusions

It's found that there is a strong correlation between higher density and smaller largest pores, which can help understand why fatigue strength increase with increasing density. For a hard, homogenous microstructure it's also found that a LEFM model can be used to correlate fatigue strength with porosity. However, for the heterogeneous structure typical for many diffusion alloyed materials crack initiation is a more complex phenomenon involving softer phases in the structure and the LEFM model is not sufficient.

References

[1] Andersson M. and Larsson M., *Linking Pore Size and Structure to the Fatigue Performance of Sintered Steels,* Proceedings of PM2010 World Congress, Florence, 2010

[2] Bergmark A., *Influence of Maximum Pore Size on the Fatigue Performance of PM Steel*, Proceedings of the International Conference DF PM 2005, editors Parilák L. and Danninger H., Stará Lesná, 2005

[3] Murakami Y., *Metal Fatigue: Effects of Small Defects and Nonmetallic Inclusions*, Elsevier, 2002

[4] Beiss P. and Lindlohr S., *Porosity Statistics and Fatigue Strength of Sintered Iron*, International Journal of Powder Metallurgy, vol. 45, Issue 2, 2009

[5] Anderson T.L., *Fracture Mechanics, Fundamentals and Applications*, 2nd edition, CRC Press, 1995

[6] MPIF Standard 56, MPIF, 2001

[7] Sonsino C.M., *Zur Bewertung des Schwingfestigkeitsverhaltens von Bauteilen mit Hilfe örtlicher Beanspruchungen*, Konstruktion, vol. 45, pp. 25-33, 1993

[8] Yu M.T. and Topper T.H., *Effect of carbon content and microstructure on near threshold crack propagation*, Int. J. Fatigue, vol 11, No 5, pp. 335-340, 1989

[9] Frost N.E., March K.J. and Pook L.P., *Metal Fatigue*, Dover Publications, 1999

[10] *Höganäs Iron and Steel Powders for Sintered Components*, Höganäs, 2002

[11] Alzati L., Bergmark A. and Andersson J., *Fatigue performance of PM steels in as-sintered state*, Proceedings of PMAI2005 in Mumbai India, 2005

[12] Svensson T., and De Maré J., *Random Features of the Fatigue Limit*, Extremes 2:2, pp 165-176, 1999

[13] Ekengren J., *Estimating inclusion content in high performance steels*, Licentiate thesis, Karlstad University Studies, 2008